



**HAL**  
open science

## Component mode synthesis methods for 3-D heterogeneous core calculations applied to the mixed-dual finite element solver MINOS

P. Guerin, Am. Baudron, J.-J. Lautard, Serge Van Criekingen

► **To cite this version:**

P. Guerin, Am. Baudron, J.-J. Lautard, Serge Van Criekingen. Component mode synthesis methods for 3-D heterogeneous core calculations applied to the mixed-dual finite element solver MINOS. Nuclear Science and Engineering, 2007, 155 (2), pp.264-275. 10.13182/NSE07-A2661 . cea-02356037

**HAL Id: cea-02356037**

**<https://cea.hal.science/cea-02356037>**

Submitted on 2 Dec 2019

**HAL** is a multi-disciplinary open access archive for the deposit and dissemination of scientific research documents, whether they are published or not. The documents may come from teaching and research institutions in France or abroad, or from public or private research centers.

L'archive ouverte pluridisciplinaire **HAL**, est destinée au dépôt et à la diffusion de documents scientifiques de niveau recherche, publiés ou non, émanant des établissements d'enseignement et de recherche français ou étrangers, des laboratoires publics ou privés.

**COMPONENT MODE SYNTHESIS METHODS FOR 3D  
HETEROGENEOUS CORE CALCULATIONS APPLIED TO THE  
MIXED DUAL FINITE ELEMENT SOLVER MINOS**

Pierre Guérin, Anne-Marie Baudron, Jean-Jacques Lautard, Serge Van Criekingen

*Commissariat à l'Energie Atomique, DEN/DANS/DM2S/SERMA/LENR, CEA Saclay*

*91191 Gif sur Yvette, France*

E-Mail: pierre.guerin@cea.fr

Total number of pages: 39

Total number of Tables: 5

Total number of Figures: 9

**Abstract** - *This paper describes a new technique for determining the pin power in heterogeneous 3D calculations. It is based on a domain decomposition with overlapping subdomains and a component mode synthesis technique for the global flux determination. Local basis functions are used to span a discrete space that allows fundamental global mode approximation through a Galerkin technique. Two approaches are given to obtain these local basis functions: in the first one (Component Mode Synthesis method), the first few spatial eigenfunctions are computed on each subdomain, using periodic boundary conditions. In the second one (Factorized Component Mode Synthesis method), only the fundamental mode is computed, and we use a factorization principle for the flux in order to replace the higher order eigenmodes. These different local spatial functions are extended to the global domain by defining them as zero outside the subdomain. These methods are well-fitted for heterogeneous core calculations because the spatial interface modes are taken into account in the domain decomposition. Although these methods could be applied to higher order angular approximations - particularly easily to a  $SP_N$  approximation - the numerical results we provide are obtained using a diffusion model. We show the methods' accuracy for reactor cores loaded with UOX and MOX assemblies, for which standard reconstruction techniques are known to perform poorly. Furthermore, we show that our methods are highly and easily parallelizable.*

## I. INTRODUCTION

Cell-by-cell homogenized transport calculations of the entire core are currently too expensive for industrial applications, even if a simplified transport ( $SP_N$ ) approximation is used. A standard technique to obtain the local pin power consists in superposing a large scale diffusion calculation with a fine mesh pre-calculated function coming from a local transport calculation. Unfortunately, this method does not work well for MOX reloaded cores due to the interface modes between UOX and MOX assemblies.

We propose here a new approach based on modal synthesis approximation. The global flux is expanded on a finite set of local basis functions obtained on overlapping subdomains. The global exact cell-by-cell problem is solved in the finite space spanned by the different local functions. We propose two methods to obtain these basis functions:

- The first one is based on the component mode synthesis (CMS, Ref. 1) method with overlapping subdomains (Ref. 2): the basis functions are several eigenfunctions (modes), solutions of a local problem on each subdomain.
- The second one computes only the fundamental mode on each subdomain, which leads to an important reduction of calculation time and memory storage. We then enlarge the basis using an asymptotic homogenization theorem on a periodic core (Ref. 3): the flux eigenfunctions are factorized as  $\varphi \approx u \times \psi$ , with  $\psi$  the rapidly varying solution of the problem on each assembly with infinite medium boundary conditions, and  $u$  the smooth shape function solution of a homogenized diffusion problem on the whole core.

We will refer to the first method as the CMS method, and to the second one as the factorized CMS (FCMS) method.

We implement here our methods in the framework of the existing MINOS solver (Ref. 4). The mixed dual finite element method is used in this solver for the resolution of the  $SP_N$  equations in 3D cartesian homogenized geometries. Even if the CMS and the FCMS methods could be applied to any angular approximation – particularly easily to a  $SP_N$  approximation, we here demonstrate their accuracy for the diffusion model. In this view, we give 2D and 3D results obtained on a 900 MWe power plant with UOX and MOX assemblies, comparing our new methods to a direct cell-by-cell calculation obtained by MINOS. The overlapping subdomains are chosen in order to capture the assembly modes as well as the interface modes. Our new solver has the advantage to be highly parallelizable, and we show its efficiency in terms of computing time and memory storage on parallel computers.

The paper is organized as follows: in Section II we recall  $SP_N$  equations and describe the MINOS solver. In Section III we introduce the CMS method; in the next one we give theoretical explanations and numerical results for the extension of this method to the mixed dual formulation of the diffusion equation. Section V is dedicated to the FCMS method and its numerical results. After the study of the parallelization efficiency of the code in Section VI, we finally conclude and give perspectives for these new methods.

## II. THE MINOS SOLVER

The MINOS solver is one of the main core computational tools of the CRONOS2 system (Refs. 4, 5). This solver is reported in the new generation neutronic system DESCARTES and has therefore been rewritten in the C++ language (Refs. 6, 7).

MINOS solves the diffusion or  $SP_N$  multigroup equations. It is based on a mixed-dual formulation of these problems. This formulation uses simultaneously scalar functions ( $\varphi_e$ ,

the even components) and vector functions ( $\vec{\varphi}_o$ , the odd components). The first even component corresponds to the scalar flux.

If  $R$  is a bounded domain with boundary  $\partial R$ , the  $SP_N$  transport equations written in the mixed (odd-even) form read as follows for each group of the multigroup equations:

$$\begin{cases} H \vec{\nabla} \varphi_e + T_o \vec{\varphi}_o = \vec{S}_o & \text{on } R \\ H^T \vec{\nabla} \cdot \vec{\varphi}_o + T_e \varphi_e = S_e & \text{on } R \\ H^T (\vec{\varphi}_o \cdot \vec{n}) = \Lambda \varphi_e & \text{on } \Gamma_1 \\ \vec{\varphi}_o \cdot \vec{n} = 0 & \text{on } \Gamma_2 \end{cases}, \quad (1)$$

where  $\varphi_e = [\varphi_0, \varphi_2, \varphi_4, \dots]^T$ ,  $\vec{\varphi}_o = [\vec{\varphi}_1, \vec{\varphi}_3, \vec{\varphi}_5, \dots]^T$ ,

$$\Gamma_1 \cup \Gamma_2 = \partial R,$$

$\Lambda$  is a full matrix associated to vacuum conditions,

$T_e$  and  $T_o$  are respectively the even and odd removal diagonal matrices:

$T_e = \text{diag}(\sigma_0, \sigma_2, \sigma_4, \dots)$  and  $T_o = \text{diag}(\sigma_1, \sigma_3, \sigma_5, \dots)$  with  $\sigma_l$  the removal cross-sections,

$H$  is a bidiagonal matrix with spatially constant coefficients coupling the odd and

even harmonics: 
$$H = \begin{bmatrix} 1 & 2 & & & & \\ & 3 & 4 & & & \\ & & 5 & 6 & & \\ & & & & \ddots & \\ & & & & & \ddots \end{bmatrix}.$$

The dual variational formulation of the  $SP_N$  equations is obtained by projecting the odd and even equations on two different functional spaces, and applying the Green formula to the odd equation. We obtain the variational problem for each group:

find  $\vec{\varphi}_o \in [H_{0,\Gamma_2}(\text{div}, R)]^{N_h}$  and  $\varphi_e \in [L^2(R)]^{N_h}$  such that

$$\begin{cases} \int_R H \varphi_e (\vec{\nabla} \cdot \vec{\psi}_o) - \int_R T_o \vec{\varphi}_o \cdot \vec{\psi}_o - \int_{\partial R} (H \Lambda^{-1} H^T) (\vec{\varphi}_o \cdot \vec{n}) (\vec{\psi}_o \cdot \vec{n}) = - \int_R \vec{S}_o \cdot \vec{\psi}_o & \forall \vec{\psi}_o \in [H_{0,\Gamma_2}(\text{div}, R)]^{N_h} \\ \int_R H^T (\vec{\nabla} \cdot \vec{\varphi}_o) \psi_e + \int_R T_e \varphi_e \psi_e = \int_R S_e \psi_e & \forall \psi_e \in [L^2(R)]^{N_h}, \end{cases} \quad (2)$$

where  $H(\text{div}, R) = \{ \vec{q} \in [L^2(R)]^S ; \vec{\nabla} \cdot \vec{q} \in L^2(R) \}$  with  $S$  the space dimension,

$$H_{0,\Gamma_2}(\text{div}, R) = \{ \vec{q} \in H(\text{div}, R), \vec{q} \cdot \vec{n} = 0 \text{ on } \Gamma_2 \},$$

$N_h$  is the number of odd and even harmonics.

More details on variational formulations and functional spaces are given in Ref. 8.

The Raviart-Thomas-Nedelec (RTN) elements (Ref. 9) are used to discretize the different functional spaces. To ensure consistency, the divergence of the vector space lies within the scalar space. Then it can be shown that the discrete solution converges to the exact continuous one. The use of these elements yields sparse matrices with coupling terms oriented only along each considered axis. Various boundary conditions can be taken into account in MINOS such as zero flux, reflection, void, albedo, translation and rotation. Discontinuity conditions on the scalar flux can also be taken into account.

### III. THE COMPONENT MODE SYNTHESIS METHOD

The CMS method for the computation of partial differential equations' eigenmodes has been used for a long time in structural analysis as well as in the asymptotic analysis of time dependent problems. This method provides a powerful tool for computing the eigenmodes of large domains thanks to its high accuracy and its high degree of parallelization. The main

idea of this method lies in the decomposition of the global structure in subdomains: a finite number of local eigenmodes of the same operator over each subdomain are chosen, and constitutes a finite basis of functions for approximating the global problem with a Galerkin method. The subdomains can be overlapping (Ref. 2) or not (Ref. 1). Here, we choose overlapping subdomains, as motivated by Ref. 2. Note that CMS with non-overlapping subdomains has already been briefly considered in Ref. 10 for the diffusion equation.

To explain the CMS method, we consider a general variational formulation of the steady state neutronic equations: find  $u_0 \in V$  and  $\lambda_0 \in \mathbb{R}$  such that

$$a(u_0, v) = \frac{1}{\lambda_0} b(u_0, v) \quad \forall v \in V, \quad (3)$$

where a and b are bilinear forms describing the problem. For the sake of simplicity we specify neither these forms nor the V space. To determine the first global eigenpair  $(u_0, \lambda_0)$ ,

we construct an overlapping subdomain decomposition of R such that:  $R = \bigcup_{k=1}^K R^k$ .

On each  $R^k$ , we consider the first  $N^k$  eigenpairs  $(u_i^k, \lambda_i^k)_{\substack{1 \leq k \leq K \\ 1 \leq i \leq N^k}}$  which are solutions of the

local problems: find  $u_i^k \in V^k$  and  $\lambda_i^k \in \mathbb{R}$  such that

$$a^k(u_i^k, v) = \frac{1}{\lambda_i^k} b^k(u_i^k, v) \quad \forall v \in V^k, \quad (4)$$

where  $a^k, b^k$  and  $V^k$  are restrictions to  $R^k$  of a, b and V respectively, with reflective boundary conditions on interfaces  $\partial R^k \setminus \partial R$ , and the actual boundary conditions on  $\partial R$ .

Now, in order to work with functions defined on the whole domain, we extend the local

solutions by zero and denote by  $\tilde{u}_i^k$  these extended functions (we explain in the next section why this extension yields conformal basis functions in our case). Then, we look for an approximate solution of problem (3) in the space spanned by all the  $\tilde{u}_i^k$  functions: find

$$\tilde{u}_0 = \sum_{k=1}^K \sum_{i=1}^{N^k} \alpha_i^k \tilde{u}_i^k \text{ and } \tilde{\lambda}_0 \in \mathbb{R} \text{ such that}$$

$$a(\tilde{u}_0, \tilde{u}_j^l) = \frac{1}{\tilde{\lambda}_0} b(\tilde{u}_0, \tilde{u}_j^l) \quad \forall 1 \leq l \leq K, 1 \leq j \leq N^l. \quad (5)$$

#### IV. EXTENSION OF THE CMS METHOD TO THE MIXED DUAL FORMULATION

We now extend the CMS method to mixed-dual variational approximations (Ref. 11). In this case, the prolongation by zero of the local functions is consistent with the different functional spaces. Indeed, the even space  $[L^2(R)]^{N_h}$  allows for discontinuous functions, thus their prolongation by zero is permissible. As for the odd space  $[H_{0,\Gamma_2}(\text{div}, R)]^{N_h}$ , conformity requires the normal trace of the odd fluxes to be continuous, and the natural way to proceed is to build local functions with reflection conditions on any subdomain boundary (except on the boundary  $\partial R$ , where the prescribed boundary conditions are always applied), and to extend them by zero outside the subdomain.

#### IV.A. Detailed presentation in the monocinetic diffusion case

Although the method we now describe remains valid in the  $SP_N$  multigroup general case, for the sake of simplicity we detail the monocinetic  $SP_1$  case with  $\vec{S}_o = 0$  (the so-called diffusion equation), using homogeneous Dirichlet boundary conditions:

$$\begin{cases} \vec{p} + D\vec{\nabla}\varphi = 0 & \text{on } R \\ \vec{\nabla}\cdot\vec{p} + \sigma_a\varphi = \frac{1}{\lambda}\sigma_f\varphi & \text{on } R, \\ \varphi = 0 & \text{on } \partial R \end{cases} \quad (6)$$

where  $D = \sigma_1^{-1}$  and  $\sigma_a = \sigma_0$ . The first equation is the so-called Fick's law. The mixed dual variational formulation of this problem is: find  $(\vec{p}, \varphi) \in H(\text{div}, R) \times L^2(R)$  and  $\lambda \in \mathbb{R}$  such that

$$\begin{cases} \int_R -\frac{1}{D}\vec{p}\cdot\vec{q} + \int_R \vec{\nabla}\cdot\vec{q}\varphi = 0 & \forall \vec{q} \in H(\text{div}, R) \\ \int_R \vec{\nabla}\cdot\vec{p}\psi + \int_R \sigma_a\varphi\psi = \frac{1}{\lambda}\int_R \sigma_f\varphi\psi & \forall \psi \in L^2(R) \end{cases} \quad (7)$$

We compute the first  $N^k$  local eigenmodes on each  $R^k$  with  $\vec{p}\cdot\vec{n}=0$  on  $\partial R_k \setminus \partial R$  (infinite medium boundary conditions), and the prescribed boundary conditions on  $\partial R$  ( $\varphi = 0$  on  $\partial R$ ): one as to find  $(\vec{p}_i^k, \varphi_i^k) \in H_{0, \partial R^k \setminus \partial R}(\text{div}, R^k) \times L^2(R^k)$  and  $\lambda_i^k \in \mathbb{R}$  such that

$$\begin{cases} \int_{R^k} -\frac{1}{D}\vec{p}_i^k\cdot\vec{q} + \int_{R^k} \vec{\nabla}\cdot\vec{q}\varphi_i^k = 0 & \forall \vec{q} \in H_{0, \partial R^k \setminus \partial R}(\text{div}, R^k) \\ \int_{R^k} \vec{\nabla}\cdot\vec{p}_i^k\psi + \int_{R^k} \sigma_a\varphi_i^k\psi = \frac{1}{\lambda_i^k}\int_{R^k} \sigma_f\varphi_i^k\psi & \forall \psi \in L^2(R^k) \end{cases} \quad 1 \leq k \leq K, 1 \leq i \leq N^k. \quad (8)$$

These local eigenmodes on each  $R^k$  extended on  $R$  by zero give global functions on  $R$  (denoted by  $\sim$ ) in the appropriate spaces, thanks to the infinite medium boundary conditions.

We define

$$\begin{aligned} W_\delta &= \text{span} \left\{ \tilde{p}_{i,d}^k \right\}_{\substack{1 \leq i \leq N^k, \\ 1 \leq d \leq K}} \subset H(\text{div}, R) \\ V_\delta &= \text{span} \left\{ \tilde{\varphi}_i^k \right\}_{\substack{1 \leq i \leq N^k, \\ 1 \leq k \leq K}} \subset L^2(R) \end{aligned} \quad , \quad (9)$$

where the subscript  $d$  denotes a given space direction: only the  $d$ -component of  $\tilde{p}_{i,d}^k$  is non zero.

The global discretized problem reads: find  $(\vec{p}_\delta, \varphi_\delta) \in W_\delta \times V_\delta$  and  $\lambda_\delta \in \mathbb{R}$  such that

$$\begin{cases} \int_R -\frac{1}{D} \vec{p}_\delta \cdot \vec{q} + \int_R \vec{\nabla} \cdot \vec{q} \varphi_\delta = 0 & \forall \vec{q} \in W_\delta \\ \int_R \vec{\nabla} \cdot \vec{p}_\delta \psi + \int_R \sigma_a \varphi_\delta \psi = \frac{1}{\lambda_\delta} \int_R \sigma_f \varphi_\delta \psi & \forall \psi \in V_\delta \end{cases} \quad . \quad (10)$$

We underline the fact that we do not require cross-section homogenization in the global problem.

Unfortunately this problem is not well-posed in the general case because the inf-sup condition for the spaces  $W_\delta$  and  $V_\delta$  is not always verified (for more explanation see Ref. 12.).

One technique to enforce this condition is to increase the number of current (odd) modes with respect to the flux (even) ones.

The unknowns of the problem (10) can be written:  $\bar{p}_\delta = \sum_{k=1}^K \sum_{i=1}^{N^k} \sum_d c_{i,d}^k \tilde{p}_{i,d}^k$  and

$\varphi_\delta = \sum_{k=1}^K \sum_{i=1}^{N^k} f_i^k \tilde{\varphi}_i^k$ , so that the following linear system in the scalar coefficients

$\{[c_{i,d}^k], [f_i^k]\}_{i=1, N^k}^{k=1, K}$  is obtained:

$$\begin{cases} -A_d [c_{i,d}^k] + B_d [f_i^k] = 0 & \forall d \\ \sum_d B_d^T [c_{i,d}^k] + T_\alpha [f_i^k] = \frac{1}{\lambda_\delta} T_f [f_i^k] \end{cases} \quad \text{with:} \quad (11)$$

$$A_d = \begin{pmatrix} A_d^{11} & A_d^{12} & \dots & A_d^{1K} \\ A_d^{21} & A_d^{22} & \dots & A_d^{2K} \\ \cdot & \cdot & \cdot & \cdot \\ A_d^{K1} & A_d^{K2} & \dots & A_d^{KK} \end{pmatrix} \quad \text{and} \quad (A_d^{kl})_{i,j} = \int_{R^k \overset{\circ}{\cap} R^l} \frac{1}{D} \tilde{p}_{i,d}^k \cdot \tilde{p}_{j,d}^l, \quad ,$$

$$B_d = \begin{pmatrix} B_d^{11} & B_d^{12} & \dots & B_d^{1K} \\ B_d^{21} & B_d^{22} & \dots & B_d^{2K} \\ \cdot & \cdot & \cdot & \cdot \\ B_d^{K1} & B_d^{K2} & \dots & B_d^{KK} \end{pmatrix} \quad \text{and} \quad (B_d^{kl})_{i,j} = \int_{R^k \overset{\circ}{\cap} R^l} \vec{\nabla} \cdot \tilde{p}_{i,d}^k \tilde{\varphi}_j^l, \quad ,$$

$$T_\alpha = \begin{pmatrix} T_\alpha^{11} & T_\alpha^{12} & \dots & T_\alpha^{1K} \\ T_\alpha^{21} & T_\alpha^{22} & \dots & T_\alpha^{2K} \\ \cdot & \cdot & \cdot & \cdot \\ T_\alpha^{K1} & T_\alpha^{K2} & \dots & T_\alpha^{KK} \end{pmatrix} \quad \text{and} \quad (T_\alpha^{kl})_{i,j} = \int_{R^k \overset{\circ}{\cap} R^l} \sigma_\alpha \tilde{\varphi}_i^k \tilde{\varphi}_j^l, \quad \sigma_\alpha = \sigma_a \text{ or } \sigma_f, \quad ,$$

where  $R^k \overset{\circ}{\cap} R^l$  is defined as the interior of  $R^k \cap R^l$ , the superscripts k and l correspond to subdomains, while the subscripts i and j correspond to eigenmodes.  $A_d$ ,  $B_d$  and  $T_\alpha$  are sparse since their constituting blocks vanish as soon as  $R^k \overset{\circ}{\cap} R^l = \emptyset$ . Moreover,  $A_d$  and  $T_\alpha$  are symmetric positive definite.

For example in the 2D case, if we denote  $\vec{p}_\delta = [p_x, p_y]^T$  and  $\varphi = \varphi_\delta$ , the global system reads: find  $(p_x, p_y, \varphi)$  and  $\lambda_\delta$  such that

$$\underbrace{\begin{bmatrix} -A_x & 0 & B_x \\ 0 & -A_y & B_y \\ B_x^T & B_y^T & T_a \end{bmatrix}}_H \begin{bmatrix} p_x \\ p_y \\ \varphi \end{bmatrix} = \frac{1}{\lambda_\delta} \begin{bmatrix} 0 & 0 & 0 \\ 0 & 0 & 0 \\ 0 & 0 & T_f \end{bmatrix} \begin{bmatrix} p_x \\ p_y \\ \varphi \end{bmatrix} \quad (12)$$

The global matrix H is sparse and symmetric but not positive definite.

#### IV.B. Application to neutronic PWR core calculations

In order to validate the method for neutronic core calculations, we use a realistic model of a PWR 900 MWe core loaded with a set of UOX and MOX assemblies (Fig. 1a). Each assembly contains 289 cells (17 in each radial direction). Fig. 1b and 1c represent the proposed decomposition of the core along four different subdivisions, yielding a total of 201 overlapping subdomains. As shown in these figures, we have chosen the internal subdomains boundaries  $\partial R_k \setminus \partial R$  on the middle of the assemblies, where the infinite medium boundary condition is believed to be close to the real value. Furthermore, with this decomposition we avoid the interface problem between UOX and MOX assemblies, because such interfaces lie within a subdomain, not on its boundary.

The implementation of the CMS method for core calculations is based on the existing  $SP_N$  MINOS solver. We present here diffusion results with two energy groups and zero-flux boundary conditions, in 2D and 3D. In the multigroup case, with g groups, one has to solve g coupled equations similar to Eq. (7), with an additional source term appearing in the right-

hand-side of the equations, due to the other groups. We always take the number of current modes larger than the number of flux modes for the above mentioned reason (inf-sup condition verified in this case).

#### *IV.C. Numerical results in 2D*

The core grid used for both direct (done by MINOS) and CMS calculations is made out of  $17 \times 17$  assemblies subdivided into  $17 \times 17$  cells. Each cell (where cross-sections are constant) is itself subdivided into 4 sub-cells. We use a  $RT_0$  approximation. This amounts to 334,084 flux unknowns. Fig. 2 gives graphical representations of the power on the whole core (2a) and of the scalar flux for the thermal (2b) and fast groups (2c).

We made two tests: 4 flux and 6 current modes on each subdomain in the first case, 9 flux and 11 current modes in the second case. Fig. 3, 4 and Table I present numerical differences between the direct MINOS calculation and our CMS method with the domain decomposition presented on Fig. 1b and 1c. As shown, we obtain a good converged and accurate calculation even with only a few modes: the  $L^2$ -Norm and the  $L^\infty$ -Norm of the power difference between the two calculations are small, and the Keff difference is smaller than 5 pcm. As could be expected, the results are better in the second case (9 flux – 11 current modes): we have more eigenfunctions in the flux and current bases, that is, the approximation spaces are bigger. Fig. 3 presents a map of the power difference between the direct MINOS calculation and our method: we can see lines parallel to the X- and Y-axis, corresponding to the jump of the flux at the interface between two subdomains. However the accuracy of the local cell power is good (Fig. 4): for 95% of the cells, the power gap between our method and the direct MINOS calculation is less than 1% in the 4 flux mode case, and less than 0.1% in the 9 flux mode case.

#### IV.D. Numerical results in 3D

The core is split into 20 planes in the Z-axis: the first and the last one are reflectors, the other ones use the same grid as in 2D (see Fig. 1a). Now we have 6,681,680 flux unknowns. We use the same domain decomposition as in 2D (Fig. 1b and 1c): we do not make a decomposition of the core in the Z-axis (the Z-size of the subdomains is equal to the one of the core).

We obtain results similar to the 2D ones, in two cases: 4 flux and 6 current modes in the first case, 8 flux and 10 current modes in the second case. The accuracy of the local cell power is satisfactory (Fig. 5): for 95% of the cells, the power gap between our method and the direct MINOS calculation is less than 1% in the 4 flux mode case, and less than 0.1% for 90% of the cells in the 8 flux mode case. The Keff difference is smaller than 10 pcm in the two cases (Table II).

### V. THE FACTORIZED COMPONENT MODE SYNTHESIS METHOD

The determination of multiple eigenfunctions on each subdomain is expensive in terms of computing time and memory storage. Our goal in this section is to perform only the fundamental mode calculation on each subdomain, and to replace the higher order modes by suitably chosen functions. The idea, coming from homogenization results, is to factorize the higher order modes (Refs. 3, 13, 14). In this view, we mention the following factorization principle proved in Ref. 3: in a periodic core, the  $i$ -th eigenmode solution of the diffusion problem (6) can be asymptotically written  $\varphi_i \approx u_i \times \psi$  with  $\psi$  the fundamental rapidly varying solution of the problem on each assembly with infinite medium boundary conditions,

and  $u_i$  the  $i$ -th smooth shape eigenfunction solution of a homogenized diffusion problem on the whole core which reads

$$\begin{cases} -\operatorname{div}(\overline{D}\nabla u) = \frac{1}{\lambda}\overline{\sigma}u \text{ on } R, \\ u = 0 \text{ on } \partial R \end{cases}, \quad (13)$$

where  $\overline{D}$  and  $\overline{\sigma}$  are homogenized constant coefficients. This reasoning remains valid for multigroup diffusion problems: the homogenized equation (13) remains monogroup.

#### *V.A. Construction of the factorized basis functions*

For a non-periodic core, we adapt the above factorization principle on each subdomain of our core decomposition. Our goal is to build basis functions that take into account the heterogeneous fine structure of the core, based only on the fundamental solutions of the local problems. First, we solve the local fine problem (8) on each subdomain, but compute only the fundamental mode  $(\vec{p}^k, \varphi^k)$ :  $N^k = 1$ . Then, we consider on each  $R^k$  the following problem derived from (13):

$$\begin{cases} -\overline{D}\Delta u_i^k = \frac{\overline{\sigma}}{\lambda}u_i^k \text{ on } R^k \\ \frac{\partial u_i^k}{\partial n} = 0 \text{ on } \partial R^k \setminus \partial R & 1 \leq k \leq K, 2 \leq i \leq N^k. \\ u_i^k = 0 \text{ on } \partial R_k \cap \partial R \end{cases} \quad (14)$$

This problem can be solved analytically: solutions are sines or cosines. We obtain our new local flux basis functions  $\tilde{\varphi}_i^k \in L^2(R)$ :

$$\begin{cases} \tilde{\varphi}_1^k = \varphi^k \text{ on } R^k \\ \tilde{\varphi}_1^k = 0 \text{ on } R \setminus R^k \\ \tilde{\varphi}_i^k = \varphi^k \times u_i^k \text{ on } R^k \\ \tilde{\varphi}_i^k = 0 \text{ on } R \setminus R^k \end{cases} \quad 1 \leq k \leq K, 2 \leq i \leq N^k. \quad (15)$$

Unfortunately, we have no such factorization property for the current. At this time we define the current basis functions in the  $d$  direction according to:

$$\begin{cases} \tilde{p}_{1,d}^k = p_d^k \text{ on } R^k \\ \tilde{p}_{1,d}^k = 0 \text{ on } R \setminus R^k \\ \tilde{p}_{i,d}^k = \frac{\partial u_i^k}{\partial d} \text{ on } R^k \quad (\text{if } \frac{\partial u_i^k}{\partial d} \neq 0) \\ \tilde{p}_{i,d}^k = 0 \text{ on } R \setminus R^k \end{cases} \quad 1 \leq k \leq K, 2 \leq i \leq N^k. \quad (16)$$

Since  $\frac{\partial u_i^k}{\partial n} = 0$  and  $\vec{p}^k \cdot \vec{n} = 0$  on  $\partial R^k \setminus \partial R$ , we have  $\tilde{p}_{i,d}^k \in H(\text{div}, R)$ .

We plan to later improve the current basis by using the factorized flux in Fick's law.

Finally, the resolution of the global system is exactly the same as in Subsection IV.A: we modify only the basis functions, replacing the higher order local eigenmodes by the functions (15) for the flux and (16) for the current.

*V.B. Numerical results in 2D*

We use here the same test case as in Subsection IV.C: same core, same grid, and same domain decomposition. In order to illustrate the determination of the smooth functions  $u_i^k$  with (14) and  $p_{i,d}^k$  with (16), we take for example an internal subdomain  $R^k$  (i.e.  $\partial R^k \cap \partial R = \emptyset$ ): we use infinite medium boundary conditions on all the boundaries of  $R^k$ . If the size of the subdomain is  $(h_x, h_y)$ , the solutions of (14) and (16) on  $R^k$  (except for a multiplicative coefficient) are:

$$\begin{cases} u_i^k = \cos\left(\frac{\pi i_x}{h_x} x\right) \cos\left(\frac{\pi i_y}{h_y} y\right) \\ p_{i,x}^k = \sin\left(\frac{\pi (i_x + 1)}{h_x} x\right) \cos\left(\frac{\pi i_y}{h_y} y\right) \\ p_{i,y}^k = \cos\left(\frac{\pi i_x}{h_x} x\right) \sin\left(\frac{\pi (i_y + 1)}{h_y} y\right) \end{cases} \quad i_x, i_y \geq 0. \quad (17)$$

Table III lists the couples of coefficients  $(i_x, i_y)$  we use, since they appear to be the best choices in our experimental results.

We present the results of the FCMS method with 6 flux and 11 current modes on each subdomain. Fig. 6, 7 and Table IV present numerical differences between the direct MINOS calculation and our FCMS method. It appears that the ratio current mode on flux mode has to be higher for the FCMS method compared to the CMS method: the determination of the current is more difficult, probably because we have no factorization technique for the current. We expect to obtain better results with an improved current basis definition, as briefly mentioned above. However, we obtain a very good accuracy in this test: the  $L^2$ -Norm and

the  $L^\infty$ -Norm of the power difference between the two solutions are small, and the Keff difference is smaller than 5 pcm (Table IV). Furthermore, for more than 97% of the cells, the power gap between our method and the direct MINOS calculation is less than 1% (Fig. 7).

In order to illustrate the need for the fundamental mode, we give in Table IV the results with only the smooth functions (17) as basis functions. It clearly appears that the results are much better with the fundamental mode than without.

### *V.C. Numerical results in 3D*

We use the same core, grid and domain decomposition as in Subsection IV.D. Since the variation of the flux in the Z-axis is small, we do not introduce a Z-dependence into  $p_{i,x}^k$  and  $p_{i,y}^k$  in (17). However, we do introduce a suitably defined  $p_{i,z}^k$ .

We choose for the numerical test 6 flux modes and 11 current modes. As shown in Table V, the FCMS method yields high accuracy. The difference with the direct MINOS calculation is very small: near 5 pcm for the Keff, the maximum power difference on the whole core is equal to 2.3%, and for more than 98% of the cells the power difference is smaller than 1% (Fig. 8).

## VI. PARALLELIZATION

The CMS and FCMS methods are easily parallelizable: each local calculation on a subdomain can be performed independently by different processes without communication. The matrix calculations need exchanges of messages, but it can also be parallelized on groups and directions. For example, in a 2-group case, if a given process does the calculation of the current matrix  $A_z$  for the fast group, this process needs to get from all the other processes the local currents for the fast group in the Z-direction, for all the subdomains.

We illustrate the efficiency of the parallelization in Fig. 9. The computer used is a 4 AMD Opteron 2.2 GHz processor server with 32 GB of shared memory. We compare the computing time between the direct MINOS calculation and our FCMS method with 1, 2 and 4 processors. We use the same numerical test as in Subsection V. C. The efficiency<sup>a</sup> of the parallel code is close to the maximum value 1 (0.85 with 2 processors, 0.8 with 4 processors). Most of the time is spent in local solves and matrix calculations. The FCMS global solve is not parallelized, but the corresponding time is very small. The computing time with our method becomes comparable to the direct MINOS calculation if 4 processors are used, and would become smaller if more processors could be used. Moreover, the code is not optimized yet, and we can expect to decrease the computation time, in particular for the matrix calculations. In terms of memory storage, the direct MINOS calculation requires about 1.7 GB for this calculation, whereas our method only needs 1.1GB.

---

## VII. CONCLUSIONS AND PERSPECTIVES

The numerical results show that the applications of the component mode synthesis method to cell-by-cell core calculations give a good accuracy for the  $K_{eff}$  as well as for the local cell power. For the same accuracy, the FCMS method based only on the fundamental mode is more efficient in terms of calculation time and memory storage than the CMS method which spends most of the computing time in determining several eigenfunctions on each subdomain. The total independence of the local mode calculations gives methods very well-fitted for parallel computers.

Presently the tests have been done only in the diffusion approximation. The next step will be to perform 3D  $SP_N$  calculations. The size of the mesh is not limited to the cell, and we can refine it for pin-by-pin calculations. Our methods could have a great interest for the calculations of future generation reactors with complex geometries, for which the mesh must be very fine (EPR, HTR, VHTR...). Another interesting application is the time dependent problems: we can keep the same basis functions for several time steps, and do only a few “updates” of the local fine functions in order to decrease the calculation time. Furthermore our methods are not related to the  $SP_N$  or diffusion models, and we intend to apply them to some transport models (the factorization principle used in the FCMS method holds true also in the transport case, see Ref. 15). Also we can consider coupling a transport or a  $SP_N$  model for local calculations, and a diffusion model for the global resolution.

In conclusion these methods offer interesting prospects for large 3D calculations with an important potential gain on parallel computers.

## FOOTNOTES

a) The efficiency of a parallel algorithm is defined by  $Eff = \frac{T_1}{N \times T_N}$ , with N the number of processors,  $T_1$  the sequential algorithm execution time and  $T_N$  the parallel one with N processors.

## REFERENCES

1. F. BOURQUIN, “Component mode synthesis and eigenvalues of second order operators: discretization and algorithm”, *M<sup>2</sup>AN*, **26**, pp. 385-423 (1992).
2. I. CHARPENTIER, F. DE VUYST and Y. MADAY, “Méthode de synthèse modale avec une décomposition de domaine par recouvrement”, *C. R. Acad. Sci. Paris*, **322**, Serie I, pp. 881-888 (1996).
3. G. ALLAIRE and Y. CAPDEBOSCQ, “Homogenization of a spectral problem in neutronic multigroup diffusion”, *Computer Methods in Applied Mechanics and Engineering*, **187**, pp. 91-117 (2000).
4. J.J. LAUTARD and F. MOREAU, “A fast 3D parallel solver based on the mixed dual finite element approximation”, *Proc. ANS Topical Mtg., Mathematical Methods and supercomputing in Nuclear Applications*, Karlsruhe, Germany, April 1993.
5. A.M. BAUDRON, J.J. LAUTARD and D. SCHNEIDER, “Mixed Dual Methods for Neutronic Reactor Core Calculations in the CRONOS System”, *Proc. ANS Topical Mtg., Mathematical Methods and supercomputing in Nuclear Applications*, Madrid, Spain, April 1999.
6. A.M. BAUDRON and J.J. LAUTARD, “Minos: a  $SP_N$  Solver for Core Calculation in the Descartes System”, *Proc. ANS Topical Mtg., Mathematical Methods and supercomputing in Nuclear Applications*, Avignon, France, September 12-15, 2005.

7. C.CALVIN, "Descartes new generation system for neutronic calculation", *Proc. ANS Topical Mtg., Mathematical Methods and supercomputing in Nuclear Applications*, Avignon, France, September 12-15, 2005.
8. H. BREZIS, *Analyse fonctionnelle, théorie et applications*, Dunod (1999).
9. P.A. RAVIART and J.P. THOMAS, *A Mixed Finite Element Method for the 2nd elliptic problems*, Lecture Notes in Mathematics, **606**, Springer Verlag, pp. 292-315 (1977).
10. K. PINCHEDEZ, "Calcul Parallèle pour les équations de diffusion et de transport homogènes en neutronique", Ph. D. Thesis, Université de Paris XI (February, 1999).
11. P.GUERIN, A.M. BAUDRON and J.J. LAUTARD, "A component mode synthesis method for 3D cell-by-cell  $SP_N$  calculation using the mixed dual finite element solver MINOS", *Proc. ANS Topical Mtg., Mathematical Methods and supercomputing in Nuclear Applications*, Avignon, France, September 12-15, 2005.
12. F.BREZZI and M.FORTIN, *Mixed and hybrid finite element method*, Springer Series in Computational Mathematics, **15**, Springer-Verlag, New York (1991).
13. J. PLANCHARD, *Méthodes mathématiques en neutronique*, Collection de la Direction des Etudes et Recherches d'Electricité de France, Eyrolles, France (1995).

14. V. SIESS, "Homogénéisation des équations de criticité en transport neutronique", Ph. D. Thesis, Université de Paris VI (January, 2004).
  
15. G. ALLAIRE and G. BAL, "Homogenization of the critically spectral equation in neutron transport", *M2AN*, **33**, pp. 721-746 (1999).

## FIGURE CAPTIONS

Fig. 1. PWR core and subdomain decomposition along four different subdivisions.

Fig. 2. Power and scalar flux representation.

Fig. 3. Graphical representation of the power gap between CMS and direct MINOS solutions in 2D.

Fig. 4. Histogram of the power cell difference between CMS and direct MINOS solutions in 2D.

Fig. 5. Histogram of the power cell difference between CMS and direct MINOS solutions in 3D.

Fig. 6. Graphical representation of the power gap between FCMS and direct MINOS solutions in 2D.

Fig. 7. Histogram of the power cell difference between FCMS and direct MINOS solutions in 2D.

Fig. 8. Histogram of the power cell difference between FCMS and direct MINOS solutions in 3D.

Fig. 9. Comparison of the computing time for a 3D calculation between FCMS method and direct MINOS calculation with 1, 2 and 4 processors.

FIGURE 1

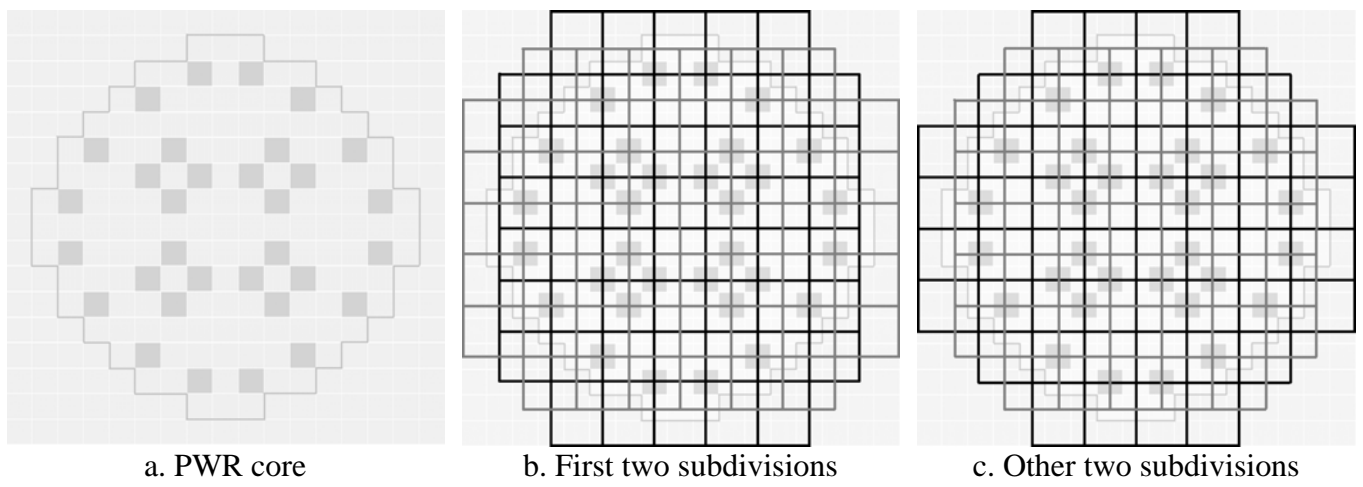


Fig. 1. PWR core and subdomain decomposition along four different subdivisions.

FIGURE 2

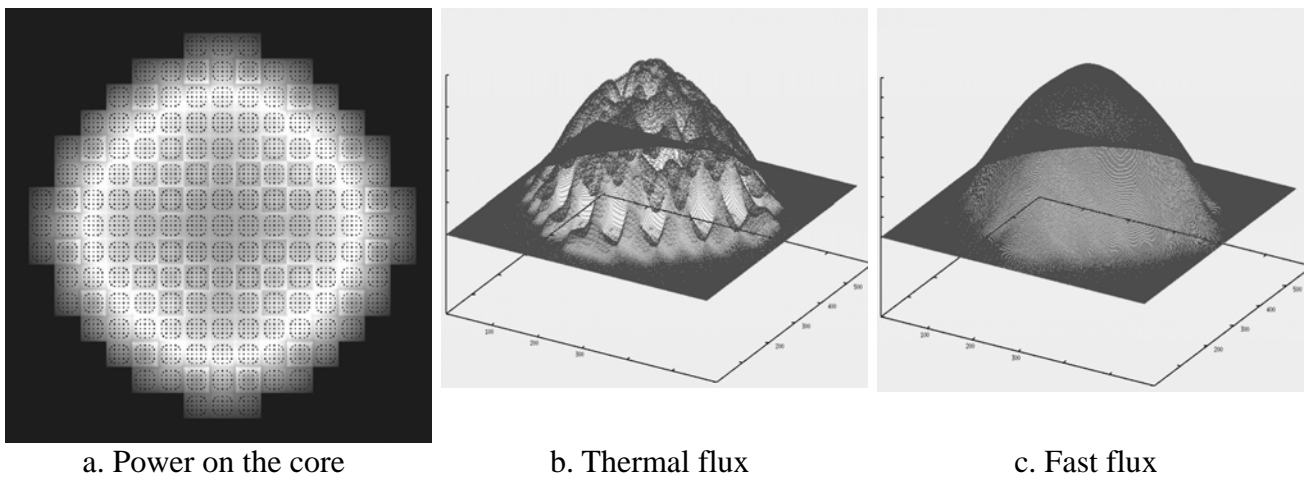


Fig. 2. Power and scalar flux representation.

FIGURE 3

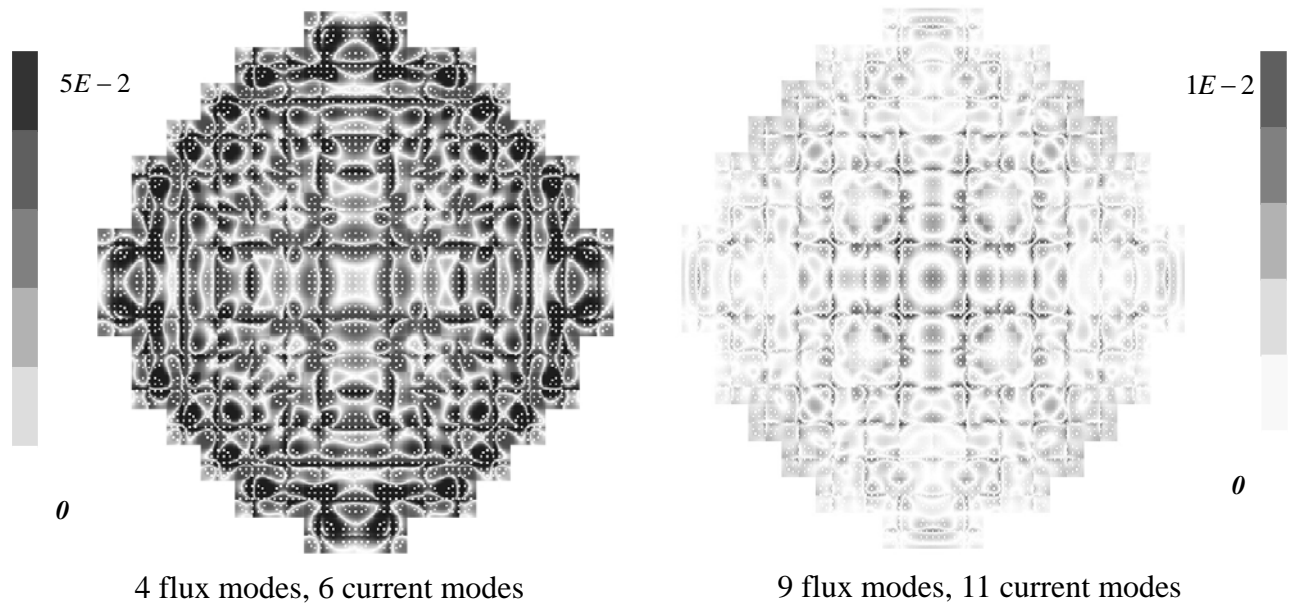


Fig. 3. Graphical representation of the power gap between CMS and direct MINOS solutions in 2D.

FIGURE 4

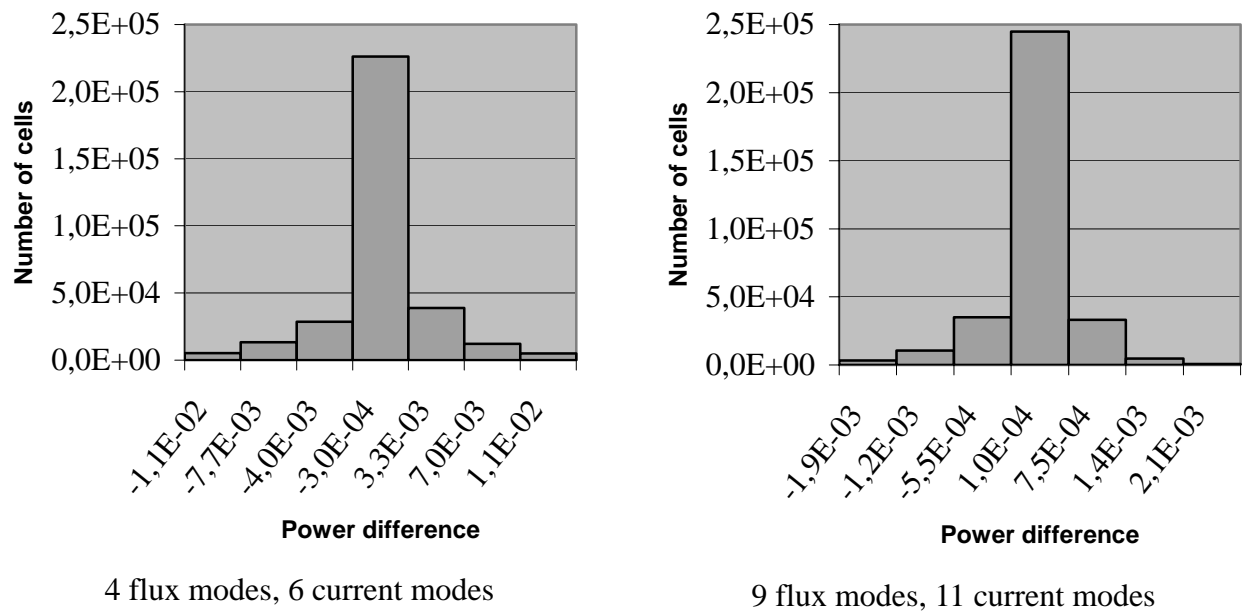


Fig. 4. Histogram of the power cell difference between CMS and direct MINOS solutions in

2D.

FIGURE 5

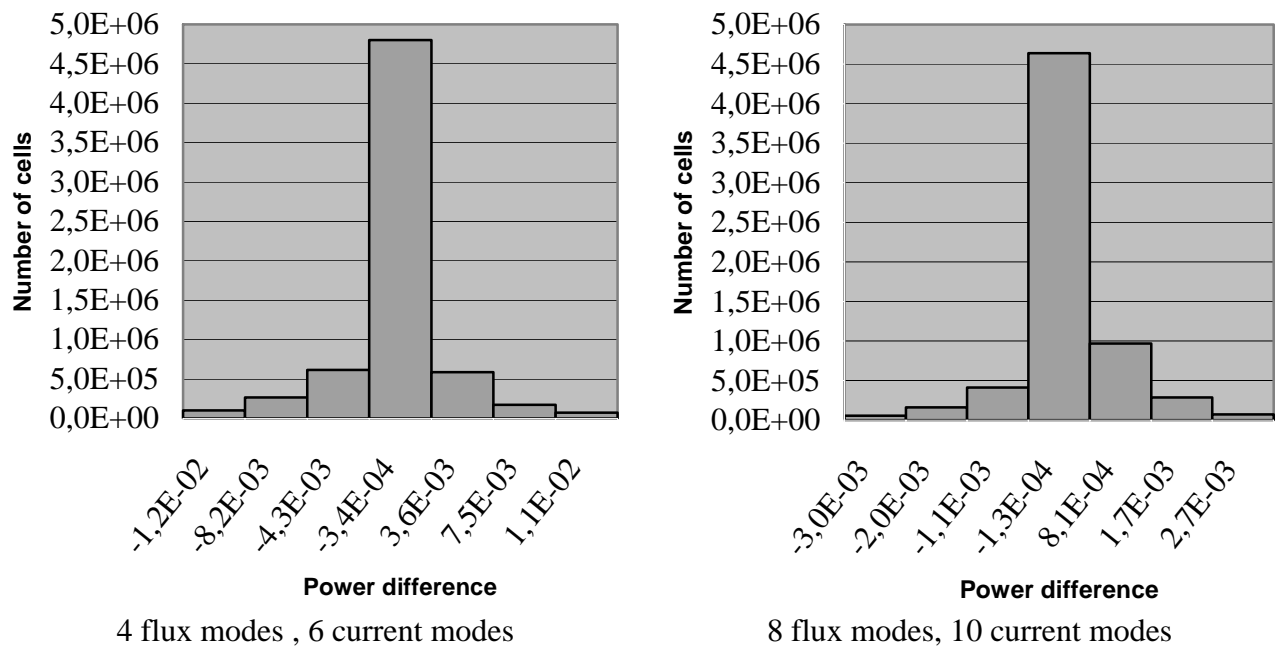


Fig. 5. Histogram of the power cell difference between CMS and direct MINOS solutions in

3D.

FIGURE 6

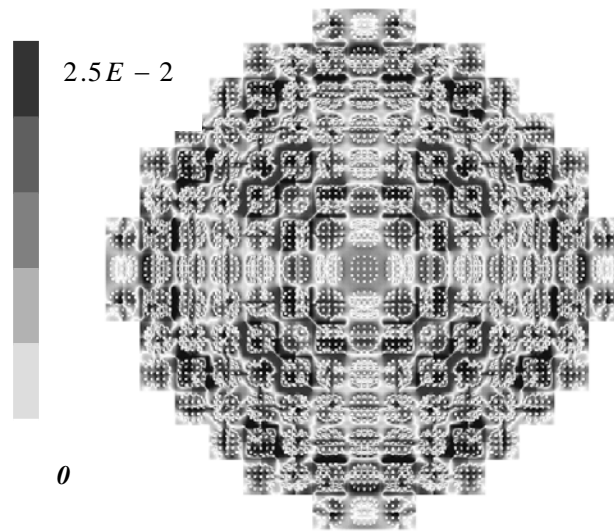


Fig. 6. Graphical representation of the power gap between FCMS and direct MINOS solutions in 2D.

FIGURE 7

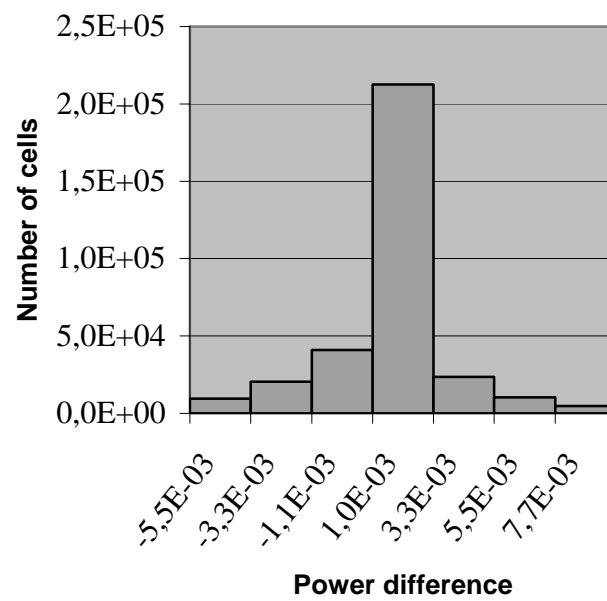


Fig. 7. Histogram of the power cell difference between FCMS and direct MINOS solutions in 2D.

FIGURE 8

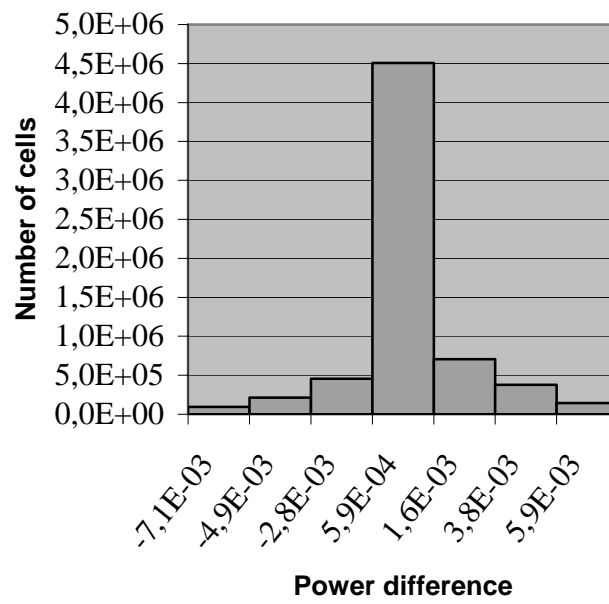


Fig. 8. Histogram of the power cell difference between FCMS and direct MINOS solutions in 3D.

FIGURE 9

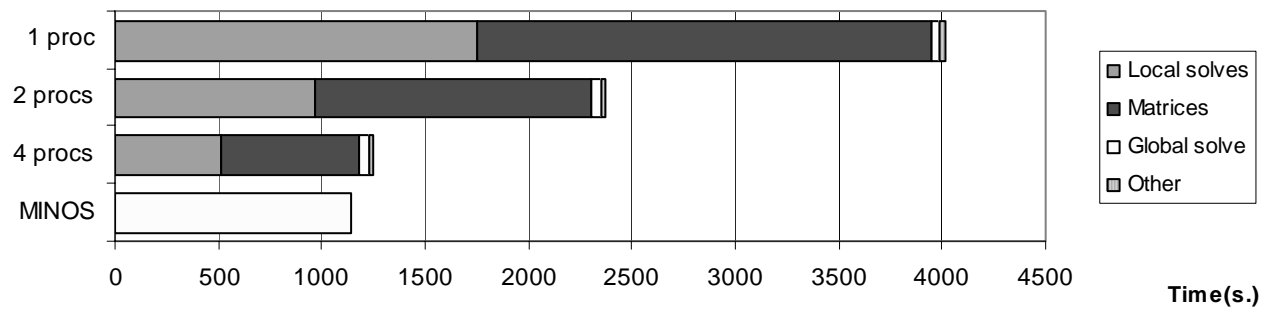


Fig. 9. Comparison of the computing time for a 3D calculation between FCMS method and direct MINOS calculation with 1, 2 and 4 processors.

Table I. Keff difference,  $L^2$  and  $L^\infty$  Norm of the power difference between CMS and direct MINOS solutions in 2D.  $K_{eff} \approx 1.180$ .

	4 flux modes, 6 current modes	9 flux modes, 11 current modes
$\Delta K_{eff}$ (pcm)	4.4	1.4
$\ \Delta P\ _2$	$3.8 \times 10^{-3}$	$5.2 \times 10^{-4}$
$\ \Delta P\ _\infty$	$5.0 \times 10^{-2}$	$9.2 \times 10^{-3}$

Table II.  $K_{eff}$  difference,  $L^2$  and  $L^\infty$  Norm of the power difference between CMS and direct MINOS solutions in 3D.  $K_{eff} \approx 1.017$ .

	4 flux modes, 6 current modes	9 flux modes, 11 current modes
$\Delta K_{eff}$ (pcm)	7.3	2.5
$\ \Delta P\ _2$	$3.7 \times 10^{-3}$	$7.9 \times 10^{-4}$
$\ \Delta P\ _\infty$	$5.1 \times 10^{-2}$	$1.0 \times 10^{-2}$

Table III. Eigenmodes indices in 2D for an internal subdomain.

$i$	$i_x$	$i_y$
1	0	0
2	1	0
3	0	1
4	2	0
5	0	2
6	1	1
7	3	0
8	0	3
9	4	0
10	0	4
11	2	2

Table IV.  $K_{eff}$  difference,  $L^2$  and  $L^\infty$  Norm of the power difference between FCMS and direct MINOS solutions in 2D. Comparison with the smooth modes only.  $K_{eff} \approx 1.180$ .

	6 flux modes, 11 current modes	Smooth modes only
$\Delta K_{eff}$ (pcm)	2.2	61
$\ \Delta P\ _2$	$2.8 \times 10^{-3}$	$1.1 \times 10^{-1}$
$\ \Delta P\ _\infty$	$2.4 \times 10^{-2}$	$8.0 \times 10^{-1}$

Table V. Keff difference,  $L^2$  and  $L^\infty$  Norm of the power difference between FCMS and directMINOS solutions in 3D.  $K_{eff} \approx 1.017$ .

	6 flux modes, 11 current modes
$\Delta K_{eff}$ (pcm)	5.77
$\ \Delta P\ _2$	$2.6 \times 10^{-3}$
$\ \Delta P\ _\infty$	$2.3 \times 10^{-2}$